Ankyrin-G-190 palmitoylation mediates dendrite and spine morphogenesis and is altered in response to lithium

Nicolas H. Piguel, Ph.D. [1,7] Sehyoun Yoon, Ph.D. [1,7] Francesca I. DeSimone, Ph.D. [2] Shaun S. Sanders, Ph.D. [2] Ruoqi Gao, Ph.D. [1] Katherine E. Horan, B.A [1] Leonardo E. Dionisio, B.A [1] , Jacob C. Garza [3] Tracey L. Petryshen, Ph.D.[3] Gareth M. Thomas, Ph.D.[4] Katharine R. Smith, Ph.D.[5] and Peter Penzes, Ph.D.[1,6,7]*

[1] Department of Physiology, Northwestern University Feinberg School of Medicine, Chicago, IL 60611

[2] Shriners Hospitals Pediatric Research Center, Lewis Katz School of Medicine at Temple University, Philadelphia, PA 19140

[3] Psychiatric and Neurodevelopmental Genetics Unit, Department of Psychiatry and Center for Genomic Medicine, Massachusetts General Hospital, Harvard Medical School, Boston, MA

[4] Shriners Hospitals Pediatric Research Center and Department of Anatomy and Cell Biology, Lewis Katz School of Medicine at Temple University, Philadelphia, PA 19140

[5] Department of Pharmacology, University of Colorado School of Medicine, Aurora, CO 80045

[6] Department of Psychiatry and Behavioral Sciences, Northwestern University Feinberg School of Medicine, Chicago, IL 60611

[7] Northwestern University Center for Autism and Neurodevelopment, Chicago, IL 60611

*Corresponding author: Department of Physiology, Northwestern University Feinberg School of Medicine, Chicago, IL 60611; Tel: 312-503-5379; p-penzes@northwestern.edu

ABSTRACT

The *ANK3* gene, encoding the protein ankyrin-G (AnkG), is associated with a variety of neuropsychiatric and cognitive disorders including bipolar disorder, autism spectrum disorder, and schizophrenia. These diseases are characterized by abnormal dendritic and synaptic architecture. AnkG is a multifunctional scaffold protein with several isoforms: The 480 kDa and 270 kDa isoforms have roles at the axon initial segment and node of Ranvier, but the function of the 190 kDa isoform (AnkG-190) is less well understood. Moreover, these isoforms are regulated by palmitoylation, but palmitoylation of AnkG-190 has not been investigated in neurons. Here we show that AnkG is required for normal dendrite and spine architecture in vivo and that AnkG-190 stabilizes pyramidal neuron dendrites. We found that Cys70 palmitoylation stabilizes AnkG-190 in spine heads and at dendritic plasma membrane nanodomains, and is necessary for the maintenance of normal spine density, dendrite arborization, and for correct microtubule dynamics. Lithium, a commonly used mood stabilizer, reverses spine and dendrite deficits induced by AnkG knockdown in a manner that is dependent of palmitoylation. Finally, we found that lithium reduces AnkG-190 palmitoylation and increases its mobility in spines. Taken together, our data reveal a novel mechanism regulating dendritic architecture and mood stabilizer action on palmitoylation of an important psychiatric disorder risk factor.

INTRODUCTION

The human *ANK3* gene, encoding the protein ankyrin-G (AnkG), has been associated with various neuropsychiatric diseases, including bipolar disorder (BD), schizophrenia, and autism spectrum disorder (1-3). Multiple independent genome wide association studies (GWAS) have strongly linked *ANK3* to BD in a variety of different ethnicities (4-7) and have been corroborated by meta-analyses (8). In addition to a genetic link with *ANK3*, some studies have shown an increase of *ANK3* expression in blood (9) and in lymphoblastoid cells of BD patients (10), revealing it as a potential biomarker. Furthermore, decreased expression of a specific AnkG isoform was observed within the cerebellum of a BD patient carrying a BD-associated *ANK3* allele (11). Thus BD risk alleles may induce both increases and decreases of *ANK3* expression, and may result in isoform-specific alterations in protein content.

Lithium is a mood stabilizer commonly used to treat BD patients as a first-line intervention (12). Responsiveness of BD patients to lithium treatment appears to be a heritable trait (13) linked to genetic markers in patients isolated from GWAS (14). The identification of 19 single nucleotide polymorphisms within the *ANK3* regulatory regions that alter the response to lithium treatment suggest that AnkG may be involved in the lithium response (15). In accordance with this, alterations in murine AnkG levels through hemizygous *Ank3* knockout (KO) (16), specific isoform KO (17) or within selected brain regions induced BD or behaviors related to schizophrenia (18). Interestingly, lithium was shown to rescue several of these behavioral deficits in AnkG KO mice (19-21).

The *ANK3* gene encodes multiple isoforms of AnkG, of which the 190, 270, and 480 kDa isoforms are the most prominent in brain (22). The giant 270 and 480 kDa isoforms have been mostly studied for their function in the axon initial segment (23) or in nodes of Ravier (24), but the 480 kDa isoform has also been shown to prevent gamma-aminobutyric acid (GABA) receptor endocytosis and to have an important role in maintaining GABAergic synapses (25). The role of the 190 kDa isoform (AnkG-190) is less fully described in neurons, but it can be found in human postsynaptic density (PSD) fractionation, where it decreases in BD (26). Moreover, AnkG-190 was found to increase in rat PSD after 5 weeks of lithium treatment (27). AnkG-190 seems to play an important role in dendritic spine maintenance and long-term potentiation through subsynaptic nanodomains in dendritic spine heads and necks (28). However, the roles of AnkG-190 in dendrite architecture, and the regulation of its localization in dendrites and synapses, are not known.

S-palmitoylation is a reversible form of post-translational modification regulating protein attachment to lipid membranes (29) and localizing proteins to different neuronal subcompartments and organelles (30). Important synaptic proteins, including neurotransmitter receptors, scaffold proteins, transporters, adhesion molecules, SNAREs, and other trafficking proteins, are palmitoylated (31). However, much less is known about the role of palmitoylation in dendrite morphogenesis and in the mechanisms of action of therapeutic agents. Notably, the membrane-binding regions of all three main AnkG isoforms harbor a cysteine residue (C70) that can be palmitoylated, a process that is required for AnkG association with the membrane, appropriate cellular localization, and function in non-neuronal cells (32, 33). Structural analysis has also shown that the membrane anchoring of AnkG is facilitated by palmitoylation, defining a stable binding interface on the lipid membrane (34). Interestingly, non-palmitoylated AnkG also localized near the membrane but lacked a unique binding interface.

Because understanding of synaptic palmitoylation is likely to provide insights into normal neuronal function but also pathophysiological and therapeutic mechanisms (35), we investigated the physiological function of AnkG palmitoylation and its roles in the actions of lithium. BD and schizophrenia are highly correlated to a decrease of dendritic spines and dendrite length in cortex (36) and in induced pluripotent stem cell (iPSC)-derived neurons (37). We show that AnkG-190 stabilizes pyramidal neuronal basal dendrites. Palmitoylation stabilizes AnkG-190 in spines and at dendritic plasma membrane nanodomains. Lithium reverses spine and dendrite deficits induced by AnkG knockdown. Finally, lithium reduces AnkG-190 palmitoylation and increases its mobility in spines. Taken together, our data reveal a novel mechanism of regulation of dendritic architecture and lithium action on the cycling of AnkG-190 palmitoylation.

METHODS

See Supplementary Methods for details.

Conditional KO mice

Ank3-floxed mice (*Ank3*$^{flox/flox}$) (The Jackson Laboratory; Bar Harbor, ME, USA; #029797) were crossed with *Camk2a*-Cre mice (The Jackson Laboratory; #005359) for forebrain-specific homozygous deletion of *Ank3* (*Ank3*$^{flox/flox}$, *Camk2a*-cre). The resulting mouse strain was called *Ank3* cKO. To maintain the colonies, *Ank3* cKO mice were mated with *Ank3*$^{flox/flox}$ mice. All experiments were performed following protocols approved by the Institutional Animal Care and Use Committee at Northwestern University.

Pharmacological treatments

2-Bromopalmitate (2-BrP), a palmitoylation inhibitor, and S-methyl methanethiosulfonate (MMTS), a thiol blocker, were from Sigma (St. Louis, MO, USA). All other chemicals were from ThermoFisher Scientific (Waltham, MA, USA) and were of the highest reagent grade. 2-BrP was used at 20 mM, palmostatin B (which inhibits depalmitoylation) at 50 µM, lithium chloride at 2 mM, and all were applied for stimulation over 24 h.

Microtubule plus-end-binding protein 3

Neurons were imaged at 37°C, 5% CO_2, with a Nikon A1R confocal microscope using a 100x oil immersion objective with NA = 1.2 in an OKOLAB stage-type CO_2 incubator. One-plan images were captured with a GaAsP detector every 2 s. Images were analyzed and kymographs were built in ImageJ, and microtubule plus-end-binding protein 3 (EB3) puncta were tracked with the plugin MTrack2.

Fluorescence recovery after photobleaching

Neurons were imaged at 37°C, 5% CO_2, with a Nikon C2 confocal microscope using a 63x oil immersion objective with NA = 1.4 in an OKOLAB stage-type CO_2 incubator. Single plane images were captured with an EMCCD camera every 10 s for 200 s. 100% laser power pulses of 1 ms (2 iterations) were used to bleach GFP in the spine. After background substation and validation of maximum 5% remaining fluorescence after photobleaching, data were normalized with the prebleach value. Recovery data points were then fitted to a one-phase association exponential in GraphPad Prism. The mobile fraction was calculated as an average of the plateaued fluorescence level and expressed as a percentage of the pre-bleached level.

RESULTS

AnkG-190 maintains dendrite complexity in pyramidal neurons

We have previously shown that AnkG-190 has an essential role in dendritic spine maintenance in vitro (28), but whether AnkG is similarly important in vivo has not been addressed. To investigate this question, we performed Golgi-Cox staining in *Ank3* cKO (*Ank3*$^{flox/flox}$, *Camk2a*-Cre) mouse brain slices. In this model, Cre recombinase is expressed under a *Camk2a* promoter to target the *Ank3* gene in the postnatal forebrain (21). We analyzed dendrites of pyramidal neurons from layer 2/3 of the somatosensory cortex, a region of the cortex where AnkG is abundant (Fig. 1a, d). Quantitative analysis of spine number showed a decrease in spine density in *Ank3* cKO brains, in support of our in vitro findings (Fig. 1c). We also observed that *Ank3* cKO mice had striking alterations in dendrite morphology with decrease in basal dendrite complexity (Fig. 1c). To specifically determine whether the effects in dendrites were cell-autonomous, we knocked down AnkG expression in rat primary cortical neurons using a previously described *Ank3* RNAi which induces a 50% decrease of AnkG staining in dendrites after 3 days of expression (28). By separating apical and basal dendrites (see supplementary methods), we again found reduced complexity in the basal dendritic arbor of AnkG knockdown pyramidal neurons (Fig. 1g), with no change in apical dendrites (Fig. 1h). Interestingly, coexpression of an RNAi-resistant AnkG-190 construct restored dendritic complexity, whereas coexpression of an RNAi-resistant 270 kDa isoform exacerbated the phenotype (Fig. 1g). Notably, AnkG knockdown also reduces dendrite complexity of interneurons, but this effect is only partially rescued by the overexpression of AnkG-270, and not at all by AnkG-190, suggesting isoform-specific requirements for different neuronal subtypes (Fig. S1a, b). Together, these data indicate that the AnkG-190 isoform may have a specific role in maintaining basal dendrite complexity in addition to maintaining spine architecture in cortical pyramidal neurons (28).

Palmitoylation of C70 stabilizes AnkG-190 in dendritic spine head and dendritic nanodomains

The specific role of AnkG-190 in dendritic spine and dendrite maintenance led us to ask what post-translational modifications can regulate these specific functions of AnkG-190. Because palmitoylation is a general mechanism for regulation of synaptic proteins, and palmitoylation of AnkG in non-neuronal cells was shown to be essential for the association of AnkG with plasma membranes (32-34), we hypothesized that this modification may also modulate AnkG's regulation in dendrites.

We first validated the presence of palmitoylated AnkG-190 in rat cortex utilizing the acyl-biotinyl exchange assay (see supplementary methods) (38), which exchanges palmitoyl modifications with biotin (Fig. 2a). We therefore mutated the palmitoylated residue (32) to alanine (C70A) in a GFP fusion construct (GFP-AnkG-190-C70A) to assess how palmitoylation-deficient AnkG-190 would behave in neuronal dendrites and spines (Fig. 2b). Confocal images revealed that overexpressed GFP-AnkG-190 was enriched in the spine head, as previously observed (28), and this enrichment was lost when C70A was mutated, matching the levels of soluble GFP (Fig. 2c, d). We then reasoned that mislocalization of palmitoylation-deficient AnkG-190 may lead to alterations in spine morphology. t. We found that while AnkG-190 expression increased spine density, as shown in Smith et al (28), GFP-AnkG-C70A had no effect on spine density (Fig. 2e, f). GFP-AnkG-190 expression also increased spine width but not length, whereas GFP-AnkG-C70A further increased both spine width and length.

To access better resolution of dendritic spines, we used super-resolution structured illumination microscopy (SIM) imaging (28, 39). SIM imaging of dendrites showed that the C70A point mutation did not alter the presence of AnkG-190 at the membrane, but changed its localization pattern (Fig. 2g). We found that AnkG-190-C70A has a more diffuse distribution pattern compared to AnkG-190 (Fig. 2h and i) measured by a smaller variation in fluorescence intensity (Puncta index), suggesting palmitoylation is important to maintain nanodomains along the dendrite. This observation suggested that palmitoylation may alter AnkG-190 mobility. To test this hypothesis, we used fluorescence recovery after photobleaching (FRAP) to measure the mobility of GFP-AnkG-190 compared with GFP-AnkG-190-C70A in dendritic spines (Fig. 2j). FRAP analysis showed that ~60% of the GFP-AnkG190 in the spine was mobile, compared with ~80% of GFP-AnkG-C70A, suggesting that preventing AnkG-190 palmitoylation increases AnkG mobility in spines (Fig. 2k, l). We also analyzed the spine content of PSD-95, which complexes with AnkG in vivo (40). Here we showed a reduction in PSD-95 accumulation in spines when we overexpressed GFP-AnkG-C70A (Fig. S2a, b), which did not affect the size of the spine compared to wild-type AnkG, as shown in the correlation profile (Fig. S2c).

AnkG-190 palmitoylation modulates dendrite complexity and microtubule dynamics

We next assessed whether palmitoylation of AnkG-190 was required to rescue the deficit in dendritic complexity in AnkG knockdown neurons. While wild-type AnkG-190 could rescue the complexity deficit in AnkG knockdown neurons in basal dendrites, coexpression with GFP-

AnkG-C70A further reduced dendritic complexity below knockdown levels (Fig. 3a-d), suggesting that the ability of AnkG-190 to be palmitoylated is important for its role in regulating dendritic arborization. Interestingly, AnkG-190-C70A affected only basal but not apical dendrites, similar to AnkG knockdown. AnkG interacts with microtubule plus-end-binding (EB) proteins EB1 and EB3, and AnkG has been directly implicated in regulating microtubule dynamics (41-43). Furthermore, microtubules are key regulators of dendritic morphogenesis in neurons (44). EB3 forms clusters at microtubule tips and can be visualized as a “comet” on polymerizing microtubules when tagged with GFP (Fig. 3e) to assess the speed of microtubule growth (43, 45), which can be represented visually with a kymograph (Fig. 3f). AnkG knockdown neurons exhibited a decrease of EB3 comet speed in dendrites compared with wild-type cells, suggesting reduced microtubule dynamics (Fig. 3g). Interestingly, AnkG knockdown induces an increase of EB3 comet speed in axon (Fig. S3). In comparison, overexpression of GFP-AnkG-190 increased EB3 comet speed compared with GFP alone (Fig. 3h). Overexpression of AnkG-190-C70A significantly reduced the speed of EB3 comets, indicating a reduction in microtubule dynamics when AnkG is unable to be palmitoylated. Collectively, these data suggest that palmitoylation of Ank-190 is required for the maintenance of normal basal dendrite arborization and for correct EB3-mediated microtubule dynamics.

Lithium rescues dendrite and spine deficits in AnkG–deficient neurons in a palmitoylation-dependent manner

Lithium has been shown to increase dendrite length in BD patients (36) and rescue spine decreases observed in iPSCs from BD patients (37). We therefore asked whether lithium could reverse dendrite and spine deficits caused by reduced AnkG expression, and what the role of palmitoylation is in this process. We treated control and AnkG knockdown neurons with lithium for 24 h and assessed spine density and morphology. As previously published, our AnkG shRNA induces a 50% decrease of AnkG immunostaining in dendrites (28). Lithium exposure rescued the dendritic spine deficits we observed in apical dendrites, causing a normalization of spine linear density and length, and also leading to a significant increase in spine width (Fig. 4a-d). Lithium failed to rescue spine deficits in the presence of 2-BrP, indicating that palmitoylation in general is necessary for the effects of lithium on these structures. Expression of GFP-AnkG-190-C70A during the treatment also prevented the rescue of spine density by lithium. Similarly, lithium rescued the deficits in dendrite arborization of basal dendrites induced by AnkG knockdown and induced a small increase in apical dendrite complexity (Fig. 4e-h). As previously observed in dendritic spines, 2-BrP and overexpression of GFP-AnkG-190-C70A prevented the

rescue by lithium. Furthermore, we also observed a small decrease in apical dendrite complexity with 2-BrP.

Together, these data show that lithium can reverse the functional effect of partial AnkG loss on dendrite and spines. We show that palmitoylation in general is required in the lithium rescue and blocking AnkG-190 palmitoylation will prevent the effects of lithium.

Lithium reduces AnkG-190 palmitoylation and increases its mobility

We wanted to further investigate the mechanisms underlying the involvement of palmitoylation in lithium-dependent rescue of different neuroarchitectural features. With the ABE assay in cortical neuron cultures followed by western blotting of AnkG-190. Interestingly, treatment with lithium resulted in a ~58% decrease in palmitoylated AnkG-190 (Fig. 5a, b). Consistent with this, immunocytochemistry of cortical neuron cultures after lithium treatment revealed a decrease in endogenous AnkG staining in mature spines (width ≥0.8 µm), which are more likely to contain AnkG (28), compared to vehicle treatment (Fig. 5c, d). These data demonstrate that lithium reduces the amount of AnkG localized in spines, which is consistent with the localization of palmitoylation-deficient AnkG. This result led us to hypothesize that lithium could prevent palmitoylation of AnkG-190 and therefore increase AnkG mobility in spines. To test this, we performed FRAP in neurons overexpressing AnkG-190 and treated with lithium for 24 h (Fig. 5e). Interestingly, lithium treatment increased the mobile fraction of AnkG-190 to ~80% compared with ~60% for controls. Furthermore, this effect was blocked by co-treatment with palmostatin B (Fig. 5f, g), suggesting that lithium may induce depalmitoylation of AnkG-190 rather than preventing its palmitoylation.

DISCUSSION

In this study, we demonstrate a role for AnkG in the arborization of pyramidal neuronal dendrites and dendritic spine density in vivo. Multiple *Ank3* KO mouse models have severe behavioral deficits related to psychiatric disorders (16, 21). Our data support that those phenotypes may, at least in part, depend on alterations of dendrite and spine architecture. Interestingly, reduced dendritic length and spine density have already been described in BD patient brain tissue in post-mortem studies (36) and in iPSCs (37). Together these observations suggest that altered neuronal morphology has an central role in neuropsychiatric diseases (46).We identify the AnkG-190 isoform as being specifically required for the cell-autonomous maintenance of basal dendrite arborization in pyramidal neurons, as the 270 kDa form is unable to rescue arborization deficits caused by knockdown of all AnkG isoforms. This phenotype can be due the specific

localization of isoforms since AnkG-190 is enriched in dendrites whereas AnkG-270 is enriched in axon (28). In addition, loss of AnkG also affects interneuron dendrites, but this dependence relies on other AnkG isoforms, indicating the cell-type specificity of AnkG-190.

We show here that AnkG-190 is palmitoylated in brain tissue, and that this modification is important for AnkG-190 subcellular localization to dendrites and spines. Unpalmitoylated AnkG has a higher mobility within spines, indicating that palmitoylation restricts its mobility to specific sites, while depalmitoylation increases the AnkG dynamics. Interestingly, loss of palmitoylation causes a selective impairment to the function of AnkG in dendritic spines; removing its ability to increase spine density, but preserving its ability to increase spine size. In contrast, mutation of AnkG's β-spectrin-binding site reduces both spine density and size (28). These data suggest that only a subset of AnkG is palmitoylated at C70A and other subpopulations of AnkG-190 exist in spines with distinct roles. We show that AnkG palmitoylation has a dendritic subcompartment-specific role, as it affects only basal but not apical dendrites. This may have implications for pathogenesis of *ANK3*-related disorders and bipolar disorder, as basal dendrites receive different inputs, integrate distinct signals, and are selectively regulated in physiological, as compared to apical ones (36, 47). Mechanistically, the role of AnkG-190 in dendritic arborization is likely related to its interaction with the microtubule plus-end-binding protein EB3. Dendrite arborization depends on microtubule growth, and AnkG has been shown to interact with EB3 in axon initial segments (41, 42). We found that AnkG knockdown and C70A mutation reduces the movement speed of EB3 puncta, consistent with reduced dendrite arborization. Knockdown of AnkG has been shown to enhance microtubule dynamics in the axon (43), which is supported by our own data, but suggests a differential role for AnkG isoforms in microtubules regulation in axons and dendrites. AnkG palmitoylation may thus increase EB3 mobility in dendrites and promote basal dendrite arborization.

Lithium is commonly used for the treatment of mood disorders and has been shown to rescue mood-related behavioral deficits in different *Ank3* KO mouse models (19-21). Studies have shown that lithium can rescue dendritic alterations in BD, suggesting a possible cellular mechanism for lithium action (36, 37). However, the cellular and molecular basis for this rescue is not well understood. In our AnkG knockdown model, we show that lithium rescues dendritic spine and dendrite arborization deficits, supporting the view that lithium acts to restore dendritic complexity in neurons, and that this may be part of its therapeutic effect. Moreover, we demonstrate that the biological process of palmitoylation in general is required for the beneficial effects of lithium on dendritic structure. However, we find that AnkG-190 palmitoylation is only

required for specific dendritic phenotypes rescued by lithium, such as the increase in spine density and basal dendrite complexity, but not for restoring spine size. Importantly, we found that lithium treatment leads to a net reduction of AnkG palmitoylation likely causing a more mobile fraction of dendritic AnkG. Based our findings we propose that dynamic palmitoylation/depalmitoylation is necessary for the normal physiological function of AnkG and the lithium-dependent rescue of neuroarchitecture. This is consistent with a report of dynamic cycling of palmitoylation of Cdc42 and other synaptic proteins, where drug-induced activity caused rapid changes in palmitoylation, indicating that cycling may be important for a role in spines (31). In addition to AnkG palmitoylation, other factors not explored here may be required for the lithium-dependent rescue of neuroarchitecture in AnkG-deficient neurons. For instance, palmitoylation of synaptic proteins such as GRIP1 or PSD-95, have been shown to regulate dendritic spines (38, 48) which may occur through a lithium-dependent re-localization (49).

In summary, we present evidence for a novel regulatory mechanism of dendritic architecture controlled by the AnkG-190 isoform which is dependent on its palmitoylation. We provide support for the cellular basis of the therapeutic actions of lithium in the *Ank3* KO mouse model, and demonstrate that this process relies on post-transcriptional palmitoylation. Our work describes a new mechanism of mood stabilizer action and its effects on an important psychiatric disorder risk factor *ANK3*. These findings open new directions for understanding basic control of neuroarchitecture, but may also provide new opportunities for treatment.

ACKNOWLEDGMENTS

This work was supported by R01MH107182 to P.P. Imaging work was performed at the Northwestern University Center for Advanced Microscopy, generously supported by NCI CCSG P30 CA060553 awarded to the Robert H. Lurie Comprehensive Cancer Center. We are grateful to members of the Penzes lab for helpful discussions, especially Dr. Marc P. Forrest for his help on the manuscript. Dr. Antonio Sanz-Clemente is gratefully acknowledged for providing access to his lab equipment. All experiments involving animals were performed according to the Institutional Animal Care and Use Committee of NU.

CONFLICT OF INTEREST

The authors declare no competing interests.

AUTHOR CONTRIBUTIONS

NHP performed and analyzed cellular and biochemical experiments, confocal imaging, SIM experiments, live imaging, Golgi staining imaging, and led the project. FID and SSS performed and analyzed the ABE assays and biochemistry. SY performed conditional knockout mouse breeding, and Golgi staining studies. RG performed biochemistry and generated neuronal cultures. KEH and LED generated and maintained neuronal cultures. JCG and TLP advised on the project. GMT supervised the ABE assays and advised on the project. KRS performed cellular experiments. PP supervised the project. All authors contributed to the writing and/or critical revision of the manuscript.

SUPPLEMENTARY INFORMATION

Supplementary information is available at MP's website.

SI consists of the following files:

Suppl Fig. S1 – PDF, representative traces of cultured rat neurons and Sholl analysis graph inhibitory neurons

Suppl Fig. S2 – PDF, SIM images of PSD-95, scatter plot showing a decrease of PSD-95 area in spine with C70A mutation, and correlation plot of spine area vs. PSD-95 area

Suppl Fig. S3 – PDF, kymographs of EB3 movement in axons from cultured rat neurons

Supplementary methods – Word

REFERENCES

1. Bi C, Wu J, Jiang T, Liu Q, Cai W, Yu P, et al. Mutations of ANK3 identified by exome sequencing are associated with autism susceptibility. Hum Mutat. 2012;33(12):1635-8.

2. Yuan A, Yi Z, Wang Q, Sun J, Li Z, Du Y, et al. ANK3 as a risk gene for schizophrenia: new data in Han Chinese and meta analysis. Am J Med Genet B Neuropsychiatr Genet. 2012;159B(8):997-1005.

3. Schulze TG, Detera-Wadleigh SD, Akula N, Gupta A, Kassem L, Steele J, et al. Two variants in Ankyrin 3 (ANK3) are independent genetic risk factors for bipolar disorder. Mol Psychiatry. 2009;14(5):487-91.

4. Scott LJ, Muglia P, Kong XQ, Guan W, Flickinger M, Upmanyu R, et al. Genome-wide association and meta-analysis of bipolar disorder in individuals of European ancestry. Proc Natl Acad Sci U S A. 2009;106(18):7501-6.

5. Smith EN, Bloss CS, Badner JA, Barrett T, Belmonte PL, Berrettini W, et al. Genome-wide association study of bipolar disorder in European American and African American individuals. Mol Psychiatry. 2009;14(8):755-63.

6. Tesli M, Koefoed P, Athanasiu L, Mattingsdal M, Gustafsson O, Agartz I, et al. Association analysis of ANK3 gene variants in nordic bipolar disorder and schizophrenia case-control samples. Am J Med Genet B Neuropsychiatr Genet. 2011;156B(8):969-74.

7. Muhleisen TW, Leber M, Schulze TG, Strohmaier J, Degenhardt F, Treutlein J, et al. Genome-wide association study reveals two new risk loci for bipolar disorder. Nat Commun. 2014;5:3339.

8. Roby Y. ANK3 gene polymorphisms and bipolar disorder: a meta-analysis. Psychiatr Genet. 2017;27(6):225-35.

9. Wirgenes KV, Tesli M, Inderhaug E, Athanasiu L, Agartz I, Melle I, et al. ANK3 gene expression in bipolar disorder and schizophrenia. Br J Psychiatry. 2014;205(3):244-5.

10. Kato T, Hayashi-Takagi A, Toyota T, Yoshikawa T, Iwamoto K. Gene expression analysis in lymphoblastoid cells as a potential biomarker of bipolar disorder. J Hum Genet. 2011;56(11):779-83.

11. Rueckert EH, Barker D, Ruderfer D, Bergen SE, O'Dushlaine C, Luce CJ, et al. Cis-acting regulation of brain-specific ANK3 gene expression by a genetic variant associated with bipolar disorder. Mol Psychiatry. 2013;18(8):922-9.

12. Malhi GS, Gessler D, Outhred T. The use of lithium for the treatment of bipolar disorder: Recommendations from clinical practice guidelines. J Affect Disord. 2017;217:266-80.

13. Grof P, Duffy A, Cavazzoni P, Grof E, Garnham J, MacDougall M, et al. Is response to prophylactic lithium a familial trait? J Clin Psychiatry. 2002;63(10):942-7.

14. Hou L, Heilbronner U, Degenhardt F, Adli M, Akiyama K, Akula N, et al. Genetic variants associated with response to lithium treatment in bipolar disorder: a genome-wide association study. Lancet. 2016;387(10023):1085-93.

15. Higgins GA, Allyn-Feuer A, Barbour E, Athey BD. A glutamatergic network mediates lithium response in bipolar disorder as defined by epigenome pathway analysis. Pharmacogenomics. 2015;16(14):1547-63.

16. Liu C, Zhang L, Wu J, Sui X, Xu Y, Huang L, et al. AnkG hemizygous mice present cognitive impairment and elevated anxiety/depressive-like traits associated with decreased expression of GABA receptors and postsynaptic density protein. Exp Brain Res. 2017;235(11):3375-90.

17. van der Werf IM, Van Dam D, Missault S, Yalcin B, De Deyn PP, Vandeweyer G, et al. Behavioural characterization of AnkyrinG deficient mice, a model for ANK3 related disorders. Behav Brain Res. 2017;328:218-26.

18. Lopez AY, Wang X, Xu M, Maheshwari A, Curry D, Lam S, et al. Ankyrin-G isoform imbalance and interneuronopathy link epilepsy and bipolar disorder. Mol Psychiatry. 2017;22(10):1464-72.

19. Leussis MP, Berry-Scott EM, Saito M, Jhuang H, de Haan G, Alkan O, et al. The ANK3 bipolar disorder gene regulates psychiatric-related behaviors that are modulated by lithium and stress. Biol Psychiatry. 2013;73(7):683-90.

20. Gottschalk MG, Leussis MP, Ruland T, Gjeluci K, Petryshen TL, Bahn S. Lithium reverses behavioral and axonal transport-related changes associated with ANK3 bipolar disorder gene disruption. Eur Neuropsychopharmacol. 2017;27(3):274-88.

21. Zhu S, Cordner ZA, Xiong J, Chiu CT, Artola A, Zuo Y, et al. Genetic disruption of ankyrin-G in adult mouse forebrain causes cortical synapse alteration and behavior reminiscent of bipolar disorder. Proc Natl Acad Sci U S A. 2017;114(39):10479-84.

22. Zhang X, Bennett V. Restriction of 480/270-kD ankyrin G to axon proximal segments requires multiple ankyrin G-specific domains. J Cell Biol. 1998;142(6):1571-81.

23. Leterrier C, Dargent B. No Pasaran! Role of the axon initial segment in the regulation of protein transport and the maintenance of axonal identity. Semin Cell Dev Biol. 2014;27:44-51.

24. Nelson AD, Jenkins PM. Axonal Membranes and Their Domains: Assembly and Function of the Axon Initial Segment and Node of Ranvier. Front Cell Neurosci. 2017;11:136.

25. Tseng WC, Jenkins PM, Tanaka M, Mooney R, Bennett V. Giant ankyrin-G stabilizes somatodendritic GABAergic synapses through opposing endocytosis of GABAA receptors. Proc Natl Acad Sci U S A. 2015;112(4):1214-9.

26. Focking M, Dicker P, Lopez LM, Hryniewiecka M, Wynne K, English JA, et al. Proteomic analysis of the postsynaptic density implicates synaptic function and energy pathways in bipolar disorder. Transl Psychiatry. 2016;6(11):e959.

27. Nanavati D, Austin DR, Catapano LA, Luckenbaugh DA, Dosemeci A, Manji HK, et al. The effects of chronic treatment with mood stabilizers on the rat hippocampal post-synaptic density proteome. J Neurochem. 2011;119(3):617-29.

28. Smith KR, Kopeikina KJ, Fawcett-Patel JM, Leaderbrand K, Gao R, Schurmann B, et al. Psychiatric risk factor ANK3/ankyrin-G nanodomains regulate the structure and function of glutamatergic synapses. Neuron. 2014;84(2):399-415.

29. Salaun C, Greaves J, Chamberlain LH. The intracellular dynamic of protein palmitoylation. J Cell Biol. 2010;191(7):1229-38.

30. Tortosa E, Hoogenraad CC. Polarized trafficking: the palmitoylation cycle distributes cytoplasmic proteins to distinct neuronal compartments. Curr Opin Cell Biol. 2018;50:64-71.

31. Kang R, Wan J, Arstikaitis P, Takahashi H, Huang K, Bailey AO, et al. Neural palmitoyl-proteomics reveals dynamic synaptic palmitoylation. Nature. 2008;456(7224):904-9.

32. He M, Jenkins P, Bennett V. Cysteine 70 of ankyrin-G is S-palmitoylated and is required for function of ankyrin-G in membrane domain assembly. J Biol Chem. 2012;287(52):43995-4005.

33. He M, Abdi KM, Bennett V. Ankyrin-G palmitoylation and betaII-spectrin binding to phosphoinositide lipids drive lateral membrane assembly. J Cell Biol. 2014;206(2):273-88.

34. Fujiwara Y, Kondo HX, Shirota M, Kobayashi M, Takeshita K, Nakagawa A, et al. Structural basis for the membrane association of ankyrinG via palmitoylation. Sci Rep. 2016;6:23981.

35. Thomas GM, Hayashi T, Huganir RL, Linden DJ. DHHC8-dependent PICK1 palmitoylation is required for induction of cerebellar long-term synaptic depression. J Neurosci. 2013;33(39):15401-7.

36. Konopaske GT, Lange N, Coyle JT, Benes FM. Prefrontal cortical dendritic spine pathology in schizophrenia and bipolar disorder. JAMA Psychiatry. 2014;71(12):1323-31.

37. Tobe BTD, Crain AM, Winquist AM, Calabrese B, Makihara H, Zhao WN, et al. Probing the lithium-response pathway in hiPSCs implicates the phosphoregulatory set-point for a cytoskeletal modulator in bipolar pathogenesis. Proc Natl Acad Sci U S A. 2017;114(22):E4462-E71.

38. Thomas GM, Hayashi T, Chiu SL, Chen CM, Huganir RL. Palmitoylation by DHHC5/8 targets GRIP1 to dendritic endosomes to regulate AMPA-R trafficking. Neuron. 2012;73(3):482-96.

39. Crosby KC, Gookin SE, Garcia JD, Hahm KM, Dell'Acqua ML, Smith KR. Nanoscale Subsynaptic Domains Underlie the Organization of the Inhibitory Synapse. Cell Rep. 2019;26(12):3284-97 e3.

40. Luoni A, Massart R, Nieratschker V, Nemoda Z, Blasi G, Gilles M, et al. Ankyrin-3 as a molecular marker of early-life stress and vulnerability to psychiatric disorders. Transl Psychiatry. 2016;6(11):e943.

41. Leterrier C, Vacher H, Fache MP, d'Ortoli SA, Castets F, Autillo-Touati A, et al. End-binding proteins EB3 and EB1 link microtubules to ankyrin G in the axon initial segment. Proc Natl Acad Sci U S A. 2011;108(21):8826-31.

42. Freal A, Fassier C, Le Bras B, Bullier E, De Gois S, Hazan J, et al. Cooperative Interactions between 480 kDa Ankyrin-G and EB Proteins Assemble the Axon Initial Segment. J Neurosci. 2016;36(16):4421-33.

43. Garza JC, Qi X, Gjeluci K, Leussis MP, Basu H, Reis SA, et al. Disruption of the psychiatric risk gene Ankyrin 3 enhances microtubule dynamics through GSK3/CRMP2 signaling. Transl Psychiatry. 2018;8(1):135.

44. Menon S, Gupton S. Recent advances in branching mechanisms underlying neuronal morphogenesis. F1000Res. 2018;7.

45. Stepanova T, Slemmer J, Hoogenraad CC, Lansbergen G, Dortland B, De Zeeuw CI, et al. Visualization of microtubule growth in cultured neurons via the use of EB3-GFP (end-binding protein 3-green fluorescent protein). J Neurosci. 2003;23(7):2655-64.

46. Forrest MP, Parnell E, Penzes P. Dendritic structural plasticity and neuropsychiatric disease. Nat Rev Neurosci. 2018;19(4):215-34.

47. Srivastava DP, Woolfrey KM, Jones KA, Anderson CT, Smith KR, Russell TA, et al. An autism-associated variant of Epac2 reveals a role for Ras/Epac2 signaling in controlling basal dendrite maintenance in mice. PLoS Biol. 2012;10(6):e1001350.

48. El-Husseini AE, Craven SE, Chetkovich DM, Firestein BL, Schnell E, Aoki C, et al. Dual palmitoylation of PSD-95 mediates its vesiculotubular sorting, postsynaptic targeting, and ion channel clustering. J Cell Biol. 2000;148(1):159-72.

49. Farooq M, Kim S, Patel S, Khatri L, Hikima T, Rice ME, et al. Lithium increases synaptic GluA2 in hippocampal neurons by elevating the delta-catenin protein. Neuropharmacology. 2017;113(Pt A):426-33.

FIGURE LEGENDS

Figure 1. The AnkG-190 isoform maintains dendrite complexity in pyramidal neurons. (**a-f**) Bright field images of Golgi-Cox staining in somatosensory cortical slices from (**a**) wild-type (WT) and (**d**) Ank3 cKO mice, scale=100 µm. Dendrite pictures (**b** and **e**, scale=5 µm) and representative traces of basal dendrites (**c** and **f**, scale=20 µm) from pyramidal neurons from cortical layer 2/3 (**g**) Scatter plot of spine density from WT and AnkG cKO mice (46 cells, 3 brains per group, t-test, ± SEM, ***p≤0.001). (**h**) Graph showing Sholl analysis for basal dendrites (20 neurons, 3 brains per group, 2-way ANOVA with Dunnett's post-test, *p≤0.05, **p≤0.01, ***p≤0.001, ±SEM. (**i**) Representative traces of cultured rat neurons expressing scramble or AnkG RNAi with GFP (no AnkG), GFP-AnkG-190, GFP-AnkG-270. Scale=100 µm. (**j-l**) Graphs showing Sholl analysis for total (**j**), basal (**k**), and apical (**l**) dendrites (15-22 neurons, 2-way ANOVA with Dunnett's post-test, *p≤0.05, **p≤0.01, ***p≤0.001, ±SEM).

Figure 2. Palmitoylation of cysteine 70 stabilizes AnkG-190 in dendritic spines and dendrites. (**a**) AnkG-190 is palmitoylated in rat forebrain. Solubilized rat forebrain homogenates were subjected to ABE to purify palmitoylated proteins. ABE fractions and a portion of input homogenate (Inp.) were western blotted to detect AnkG. Exclusion of NH_2OH was used as a control for assay specificity. (**b**) Schematic of 190 kDa Ankyrin-G isoform showing the mutated cysteine which prevents palmitoylation. (**c**) Confocal images of cultured cortical neurons expressing mCherry with GFP, GFP-AnkG-190, or GFP-AnkG-190-C70A, scale=5 µm. (**d**) Linescan analysis of spine:dendrite ratio of expressed GFP, GFP-AnkG-190, or GFP-AnkG-190-C70A (16-20 neurons per condition, 2-way ANOVA with Dunnett's post-test, ***p≤0.001, ±SEM). (**e**) Confocal images of cultured cortical neurons expressing mCherry with GFP, GFP-AnkG-190, or GFP-AnkG-190-C70A, scale=5 µm. (**f**) Scatter plots showing quantification of spine density, spine width, and spine length for neurons in (e) (n=19-22 neurons, 1-way ANOVA with a Dunnett's post-test, *p≤0.05, **p≤0.01, ***p≤0.001, ±SEM). (**g**) Spine SIM imaging 3D reconstruction of cultured rat neurons expressing mCherry (white), GFP-AnkG-190 or GFP-AnkG-190-C70A (both green), and immunostained for PSD-95 (pink). (**h**) SIM imaging of dendrites from cultured cortical neurons expressing GFP-AnkG-190 or GFP-AnkG-190-C70A, scale=0.5 µm, in gray or pseudocolor (middle and bottom) and their associated normalized linescan (top). (**i**) Scatter plot of the puncta index average (7-9 neurons per condition, Mann Whitney, *p≤0.05, ±SEM) for GFP-AnkG-190 or GFP-AnkG-190-C70A overexpression. (**j**) Representative time lapse images of GFP-AnkG-190 and GFP-AnkG-190-C70A during a FRAP

experiment, scale=2 µm. (**k**) Quantification of GFP fluorescence in spines over time. Data are fitted with single exponentials (colored lines). Data are represented as mean ±SEM. (**l**) Scatter plot of mobile fraction (left) or half time recovery (right) of GFP-AnkG-190 and GFP-AnkG-190-C70A (n=15-22 neurons, ANOVA with Dunnett's post-test, ***p≤0.001, ±SEM).

Figure 3. AnkG-190 palmitoylation modulates basal dendrite complexity and microtubule dynamics (**a**) Representative traces of cultured rat neurons expressing AnkG RNAi with GFP-AnkG-190 or GFP-AnkG-190-C70A for three days, scale=100 µm. (**b-d**) Graphs showing Sholl analysis for total (**b**), basal (**c**), and apical (**d**) dendrites (15 to 22 neurons, 2-way ANOVA with Dunnett's post-test, *p≤0.05, **p≤0.01, ***p≤0.001, ±SEM). (**e**) Representative time lapse images of dendrites from cultured rat neurons expressing EB3-dtTomato for three days. (**f**) Annotated kymograph. (**g-h**) Representative kymographs of dendrites from neurons expressing for three days: EB3-tdTomato plus either scramble or AnkG RNAi (**g**), EB3-tdTomato plus GFP, GFP-AnkG-190, or GFP-AnkG-190-C70A (**h**). (**i**) Scatter plots showing EB3-GFP speed of movement in the presence of scramble or AnkG RNAi (top, n=10-13 neurons, t-test, **p≤0.01, ±SEM), or in the presence of GFP, GFP-AnkG-190, or GFP-AnkG-190-C70A overexpression (bottom, n=10-12 neurons, 1-ANOVA with Dunnett's post-test, *p≤0.05, **p≤0.01, ±SEM).

Figure 4. Lithium treatment rescues the spine and dendrite deficit in AnkG knockdown neurons and requires palmitoylation. (**a**) Confocal images of mCherry from cultured rat neurons transfected for three days with scramble or AnkG RNAi and treated with lithium chloride +/- 2-bromopalmitate, scale=10 µm. (**b-d**) Scatter plots showing spine density, spine length, and spine head width (21-30 neurons, Kruskal-Wallis with Dunnett's post-test, *p≤0.05, **p≤0.01, ***p≤0.001, ±SEM). (**e**) Representative traces of cultured rat neurons expressing scramble or AnkG RNAi, +/- lithium chloride and 2-bromopalmitate, scale=100 µm. (**f-h**) Sholl analysis graph for total, basal, and apical dendrites (27 to 74 neurons, 2-way ANOVA with Dunnett's post-test, *p≤0.05, **p≤0.01, ***p≤0.001, ±SEM).

Figure 5. Lithium induces a decrease of palmitoylated AnkG-190 isoform and increases its mobility. (**a**) Lysates of cortical neurons treated with the indicated compounds were subjected to ABE to purify palmitoylated proteins. Levels of palmitoyl-AnkG-190 (top blot) and total AnkG expression in parent lysates (bottom blot) were detected with specific antibodies. Exclusion of NH_2OH was used as a control for assay specificity. (**b**) Bar graph of 190 kDa AnkG isoform palmitoylation normalized with the input and relative to the untreated condition (5

independent experiments, t-test, *p≤0.05, ±SEM). (**c**) Representative maximal projection of confocal image of endogenous AnkG staining in cortical neurons transfected with GFP with or without lithium stimulation, scale=2 µm. (**d**) Scatter plot of AnkG mean intensity in mushroom spines on a single plane (26-30 neurons on 3 independent experiments, t-test, ***p≤0.001, ±SEM). (**e**) Representative time lapse images of GFP-AnkG-190 with lithium chloride +/- palmostatin B in FRAP experiments, scale=2 µm. (**f**) Quantification of GFP fluorescence in spines over time. Data are fitted with single exponentials (colored lines). Data are represented as mean ±SEM. (**g**) Scatter plots of mobile fraction (left) or half time recovery (right) of GFP-AnkG-190 in the presence of lithium chloride +/- palmostatin B (n=15-22 neurons, 1-ANOVA with Dunnett's post-test, ***p≤0.001)

Figure 1

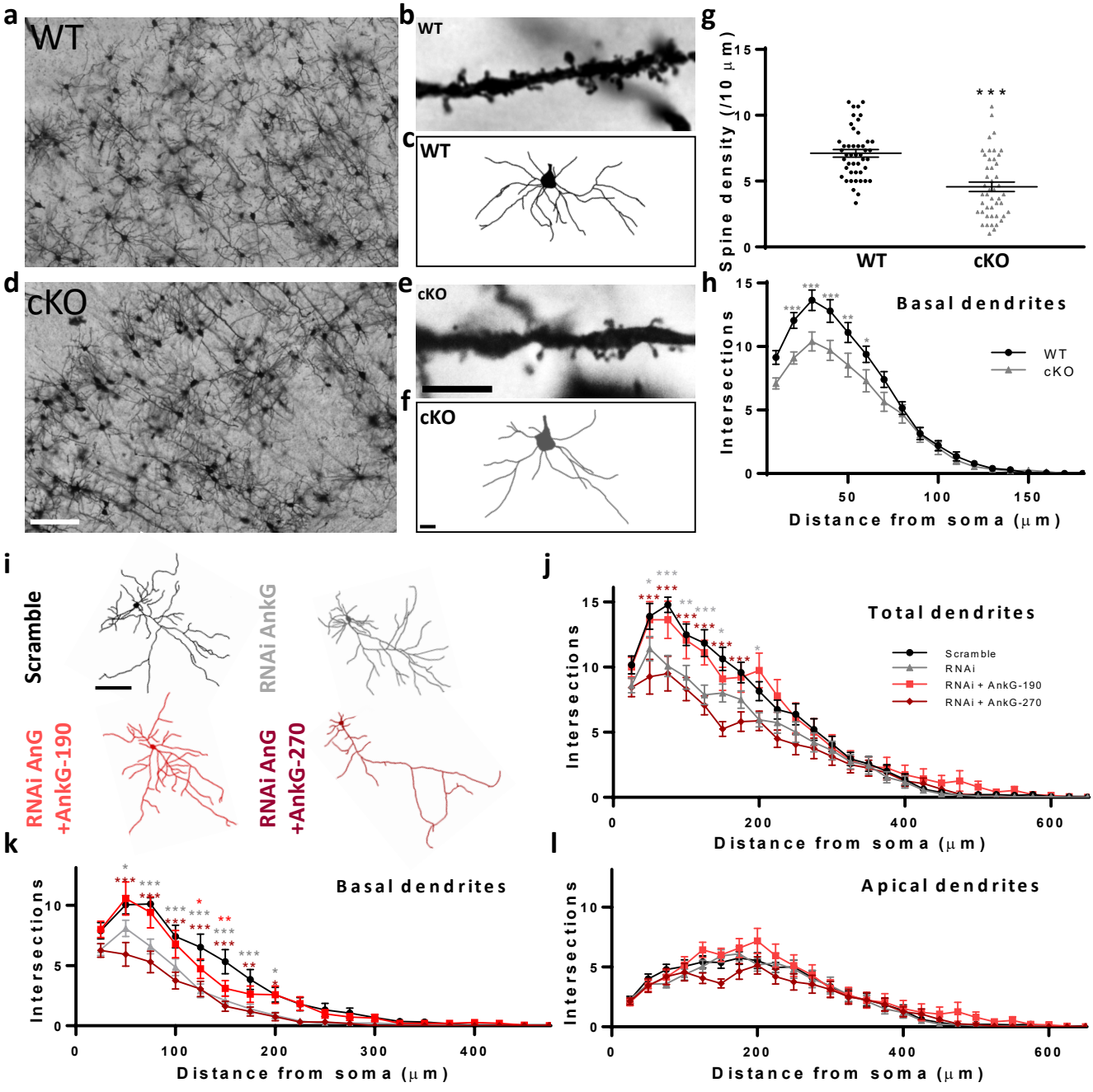
a
WT
b
WT
c
WT
d
cKO
e
cKO
f
cKO
g
Spine density (/10 μm)
***
WT
cKO
h
Basal dendrites
Intersections
WT
cKO
Distance from soma (μm)
i
Scramble
RNAi AnkG
RNAi AnG +AnkG-190
RNAi AnG +AnkG-270
j
Total dendrites
Intersections
Scramble
RNAi
RNAi + AnkG-190
RNAi + AnkG-270
Distance from soma (μm)
k
Basal dendrites
Intersections
Distance from soma (μm)
l
Apical dendrites
Intersections
Distance from soma (μm)

Figure 2

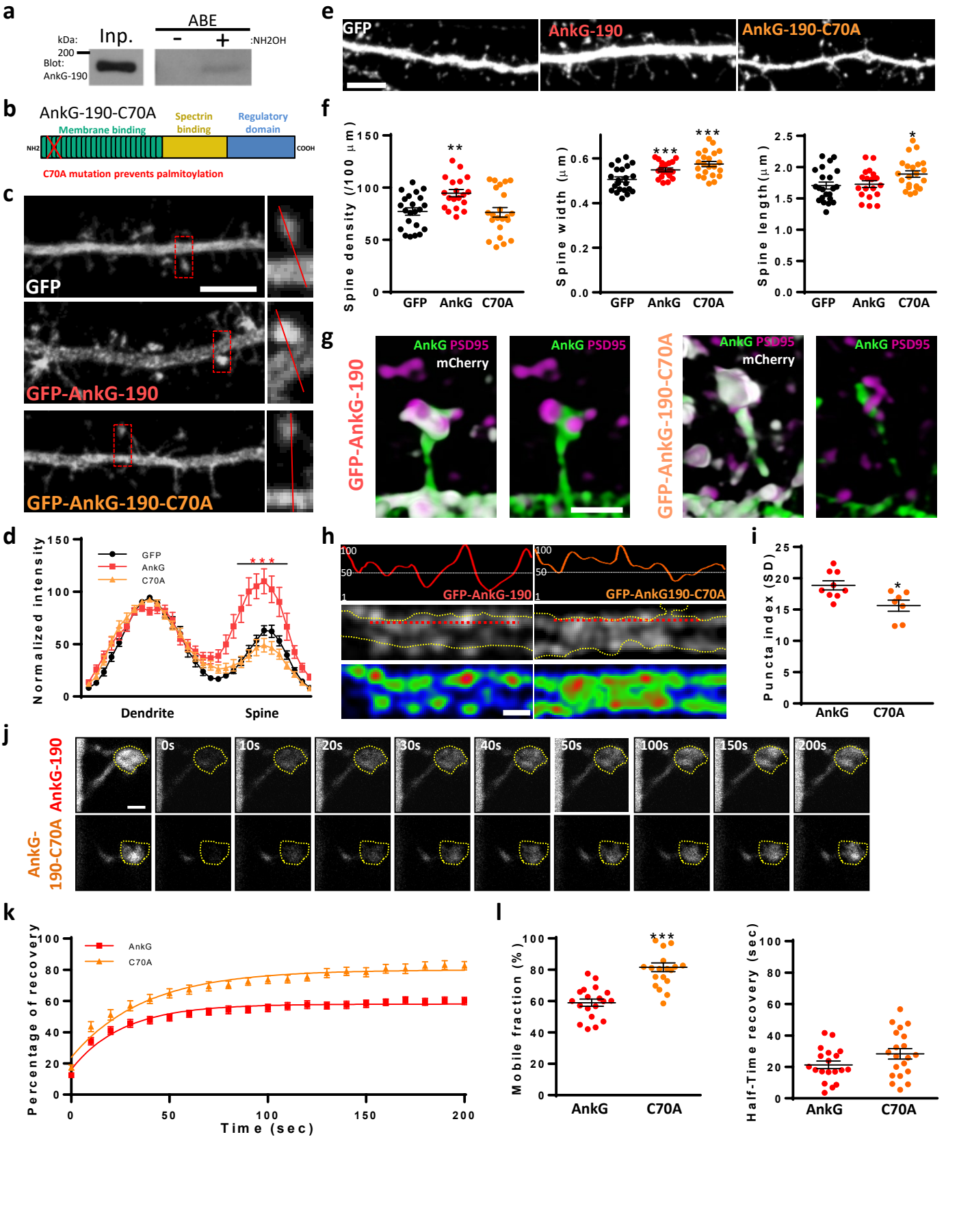
a
ABE
kDa:
Inp.
-
+
:NH2OH
200
Blot:
AnkG-190
b
AnkG-190-C70A
Membrane binding
Spectrin binding
Regulatory domain
NH2
COOH
C70A mutation prevents palmitoylation
c
GFP
GFP-AnkG-190
GFP-AnkG-190-C70A
d
Normalized intensity
GFP
AnkG
C70A
***
Dendrite
Spine
e
GFP
AnkG-190
AnkG-190-C70A
f
Spine density (/100 μm)
**
GFP
AnkG
C70A
Spine width (μm)
***
Spine length (μm)
*
g
GFP-AnkG-190
GFP-AnkG-190-C70A
AnkG PSD95
mCherry
h
GFP-AnkG-190
GFP-AnkG190-C70A
i
Puncta index (SD)
AnkG
C70A
j
AnkG-190
AnkG-190-C70A
0s
10s
20s
30s
40s
50s
100s
150s
200s
k
Percentage of recovery
Time (sec)
l
Mobile fraction (%)
Half-Time recovery (sec)

Figure 3

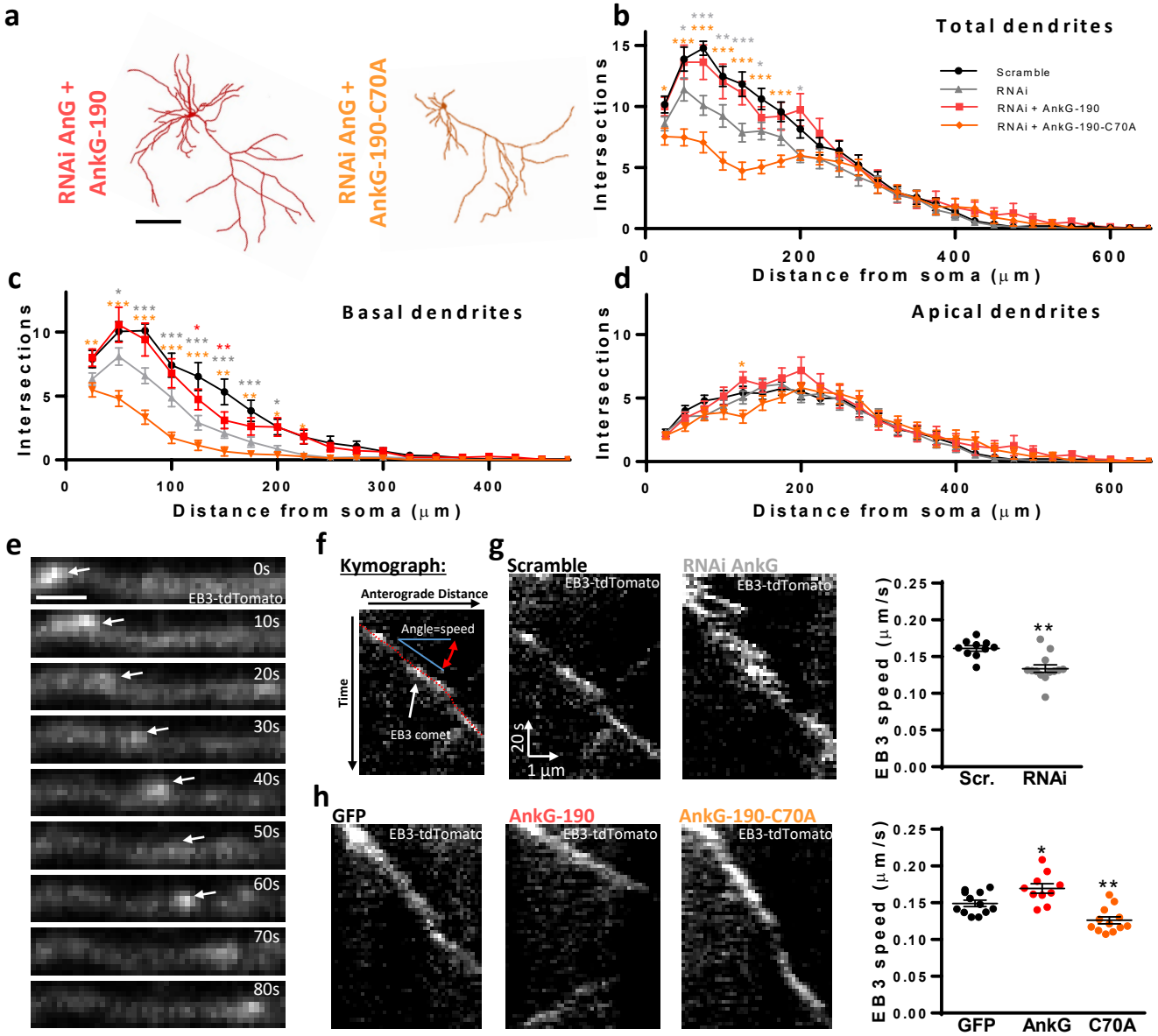
a
RNAi AnG + AnkG-190
RNAi AnG + AnkG-190-C70A
b
Total dendrites
Scramble
RNAi
RNAi + AnkG-190
RNAi + AnkG-190-C70A
Intersections
Distance from soma (μm)
c
Basal dendrites
Intersections
Distance from soma (μm)
d
Apical dendrites
Intersections
Distance from soma (μm)
e
0s
10s
20s
30s
40s
50s
60s
70s
80s
EB3-tdTomato
f
Kymograph:
Anterograde Distance
Angle=speed
Time
EB3 comet
g
Scramble
RNAi AnkG
EB3-tdTomato
20 s
1 μm
EB3 speed (μm/s)
Scr.
RNAi
h
GFP
AnkG-190
AnkG-190-C70A
EB3-tdTomato
EB3 speed (μm/s)
GFP
AnkG
C70A

Figure 4

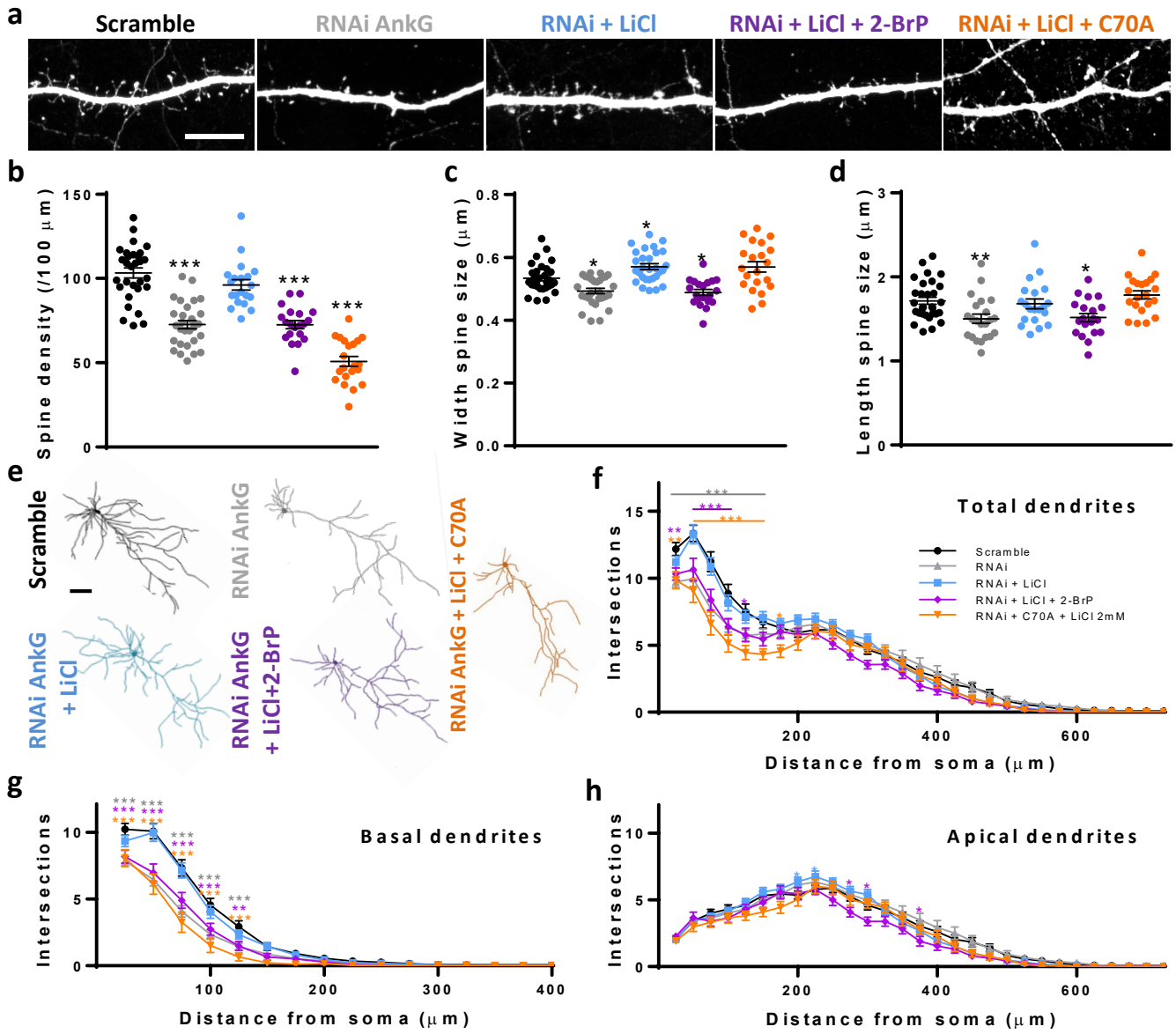
a
Scramble
RNAi AnkG
RNAi + LiCl
RNAi + LiCl + 2-BrP
RNAi + LiCl + C70A
b
Spine density (/100 µm)
c
Width spine size (µm)
d
Length spine size (µm)
e
Scramble
RNAi AnkG
RNAi AnkG + LiCl
RNAi AnkG + LiCl+2-BrP
RNAi AnkG + LiCl + C70A
f
Total dendrites
Intersections
Distance from soma (µm)
Scramble
RNAi
RNAi + LiCl
RNAi + LiCl + 2-BrP
RNAi + C70A + LiCl 2mM
g
Basal dendrites
Intersections
Distance from soma (µm)
h
Apical dendrites
Intersections
Distance from soma (µm)

Figure 5

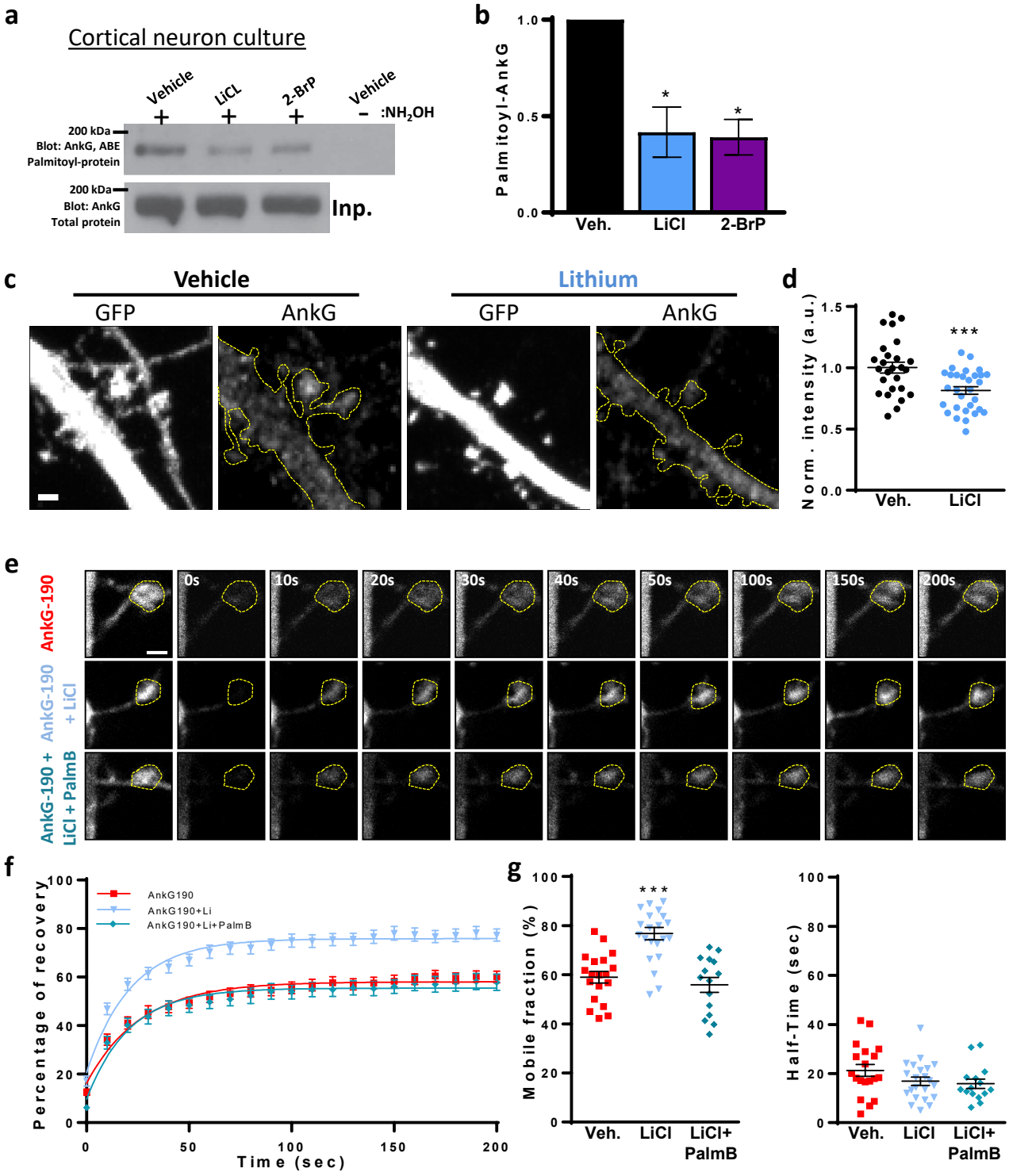
a
Cortical neuron culture
Vehicle
LiCl
2-BrP
Vehicle
+
+
+
– :NH2OH
200 kDa
Blot: AnkG, ABE
Palmitoyl-protein
200 kDa
Blot: AnkG
Total protein
Inp.
b
Palmitoyl-AnkG
1.0
0.5
0.0
*
*
Veh.
LiCl
2-BrP
c
Vehicle
Lithium
GFP
AnkG
GFP
AnkG
d
Norm. intensity (a.u.)
1.5
1.0
0.5
0.0
***
Veh.
LiCl
e
AnkG-190
AnkG-190 + LiCl
AnkG-190 + LiCl + PalmB
0s
10s
20s
30s
40s
50s
100s
150s
200s
f
Percentage of recovery
100
80
60
40
20
0
AnkG190
AnkG190+Li
AnkG190+Li+PalmB
0
50
100
150
200
Time (sec)
g
Mobile fraction (%)
100
80
60
40
20
0
***
Veh.
LiCl
LiCl+ PalmB
Half-Time (sec)
100
80
60
40
20
0
Veh.
LiCl
LiCl+ PalmB